Received: 20 March 2024 | Revised: 25 April 2024 | Accepted: 11 May 2024

DOI: 10.1002/asl.1253

RESEARCH ARTICLE

Atmospheric Science Letters RMetS

Assessing the extended-range forecast skills of the extreme heat events over South China based on three S2S models

Xiaoqi Li[1] | Ruidan Chen[1,2] | Yunting Qiao[1,2]

[1]School of Atmospheric Sciences and Guangdong Province Key Laboratory for Climate Change and Natural Disaster Studies, Sun Yat-Sen University, and Southern Marine Science and Engineering Guangdong Laboratory (Zhuhai), Zhuhai, China

[2]Key Laboratory of Tropical Atmosphere–Ocean System, Ministry of Education, Zhuhai, China

Correspondence
Ruidan Chen, School of Atmospheric Sciences and Guangdong Province Key Laboratory for Climate Change and Natural Disaster Studies, Sun Yat-sen University, and Southern Marine Science and Engineering Guangdong Laboratory (Zhuhai), Zhuhai, China.
Email: chenrd3@mail.sysu.edu.cn

Funding information
Joint Funds of the National Natural Science Foundation of China, Grant/Award Number: U2342205; National Natural Science Foundation of China, Grant/Award Number: 42375028; Innovation Group Project of Southern Marine Science and Engineering Guangdong Laboratory (Zhuhai), Grant/Award Number: 316323005; Science and Technology Planning Project of Guangdong Province, Grant/Award Number: 2023B1212060019

Abstract

This paper assesses the extended-range forecast skills of the extreme heat events (EHEs) over South China based on three subseasonal-to-seasonal models (European Centre for Medium-Range Weather Forecasts [ECMWF], National Centers for Environmental Prediction [NCEP], and China Meteorological Administration [CMA]). Overall, ECMWF has the best skill, NCEP the second and CMA the poorest. The predicting skills of EHEs depend on the predicting skills of relevant circulation. Cases studies (June 4–6, 1999, August 19–29, 2009, and August 3–5, 2010) show that the three models generally predict circulation anomalies weaker than observation, leading to the misses of some extreme heat days (EHDs). In these cases, ECMWF is able to well predict the influence of tropical circulation, capture the major characteristics of mid-latitude circulation but with a slower propagating speed. NCEP could capture the main signals of tropical (mid-latitude) circulation, but with slower propagating speed (slower propagating speed, deviated direction or more northward location). CMA might produce some EHDs but is derived from the circulation anomaly with the wrong origin or location. Therefore, ECMWF could predict the EHEs most accurately, NCEP could reasonably predict the formation of EHEs and tend to have more delayed predictions, while CMA has the poorest skill due to the false origins of anomalies. These results suggest potential ways to improve the current models' extended-range forecast skills.

KEYWORDS

atmosphere, geophysical sphere, physical phenomenon, severe weather, weather and climate prediction, weather/climate extremes

1 | INTRODUCTION

Extreme heat events (EHEs) occur frequently under global warming, which causes great threats to society and has become a research focus (Chen & Lu, 2015; IPCC, 2023; Wang et al., 2023; Weaver et al., 2014; Zheng and Wang 2019). South China is a hotspot of EHEs in China and is facing great pressure in dealing with the associated disasters, considering its dense population. Therefore, further studies are needed to advance the forecast skills of the EHEs in South China. Compared with short-term weather forecasts and long-term climate

predictions, the extended-range forecast in between is currently the biggest challenge (White et al., 2022; Zhang et al., 2019). Improving the extended-range forecast skills of EHEs is critical for early warning, which could help reduce risks and ensure people's production and life.

One way to perform extended-range forecasts is using statistical models (Gao et al., 2018; Hsu et al., 2015; Li et al., 2023). For instance, Zhu and Li (2018) attempted to build a spatiotemporal projection model to forecast the summer temperature and EHEs over China at 5–30 days leads. Another approach to extended-range forecast is using numerical dynamical models. To improve the prediction at subseasonal-to-seasonal (S2S) timescales, the World Weather Research Program and World Climate Research Program jointly launched the S2S prediction project (Vitart et al., 2017), providing reforecast data to evaluate the prediction skills of different dynamic models. Many studies have evaluated the extended-range forecast skills of EHEs based on S2S models (Lin, Mo, et al., 2022; Vitart & Robertson, 2018; Wulff & Domeisen, 2019). For China, relevant research mainly focused on the Yangtze River basin (Qi & Yang, 2019; Yang et al., 2018; Zhang et al., 2024). Xie et al. (2020) compared the performance of three S2S models in the extended-range forecasts of the EHEs over the Yangtze River basin and indicated that the model with better forecast skill could reasonably capture the EHEs at 10-day leads. The bias in intraseasonal circulation anomalies is regarded as an important bias source in the forecast of EHEs (Qi & Yang, 2019; Xie et al., 2020).

In this study, we assess the extended-range forecast skills of the EHEs over South China based on S2S models, which have not yet been carried out. The causes of the models' different skills are investigated by comparing the circulation evolution between the observation and models. Section 2 describes the data and methods. Section 3 presents the overall assessment of the forecast skills and explains the models' different performance based on cases. Section 4 gives the conclusions.

2 | DATA AND METHODS

T_{max} is extracted from the CN05 (V2.0) dataset provided by the National Climate Center in China, which is based on the observation over 2472 stations and interpolated onto a horizontal resolution of 0.5° × 0.5° (Xu et al., 2009). Daily circulation data are obtained from the National Centers for Environmental Prediction and National Center for Atmospheric Research (NCEP–NCAR) reanalysis datasets, with a horizontal resolution of 2.5° × 2.5° (Kalnay et al., 1996). The reforecast data of three models from the European Centre for Medium-Range Weather Forecasts (ECMWF), the NCEP, and the China Meteorological Administration (CMA) are downloaded from the S2S database server. The data in summer during the common period of these three models (1999–2010) is extracted for analyses. The model details are listed in Table S1. Because the NCEP and CMA models produce the forecast every day while ECMWF twice a week, we apply a data processing method proposed by previous studies (Xie et al., 2020; Yang et al., 2018) to reprocess the ECMWF data to daily data. Specifically, the forecasts from $N-2$ to $N+2$ days are used to represent the results of the N-day lead forecast, and if there are two values in a specific lead time forecast, then their arithmetic average is adopted. After reprocessing, the reforecast data of the ECMWF model starts from a 3-day lead.

An extreme heat day (EHD) is defined when the average T_{max} over South China (18° N–28° N, 105° E–120° E; Figure 1) exceeds the 90th percentile of its climatological time series during the 15-day moving window centered on the identical calendar day. Considering the climatological cold biases over South China in models (Figure 1a–d), the 90th percentile thresholds are calculated separately for the observation and each model's ensemble mean. The anomalies in EHDs in the observation and each model are gained by subtracting their own daily climatology. The three models also underestimate the T_{max} variability (Figure 1e–h), contributing to the systematic errors of smaller T_{max} anomalies in the models. An EHE is defined as at least three consecutive EHDs occur. According, there are a total of 17 EHEs and 113 EHDs in the observation. For the model prediction, an EHE is regarded as correctly predicted when at least half of the EHDs during the event are hit.

The Heidke skill score (HSS) (Heidke, 1926), which ranges from $-\infty$ to 1 with positive values closer to 1 meaning better skills, is adopted to evaluate the model's hit rate of EHDs. The probability of detection, false alarm rate, and miss rate are also employed to assess the deterministic forecast skills across the models. The detailed calculations of the above statistical metrics are described in the Supporting Information.

3 | RESULTS

3.1 | Overall assessment of the forecast skills

Figure 2 shows the models' forecast scores for forecasting the EHDs over South China at different lead times. The ensemble forecasts are better than individual members. Thus, only the ensemble forecast skills are analyzed. Overall, the ECMWF model performs the best for all four metrics, NCEP the second, and CMA the worst. Taking

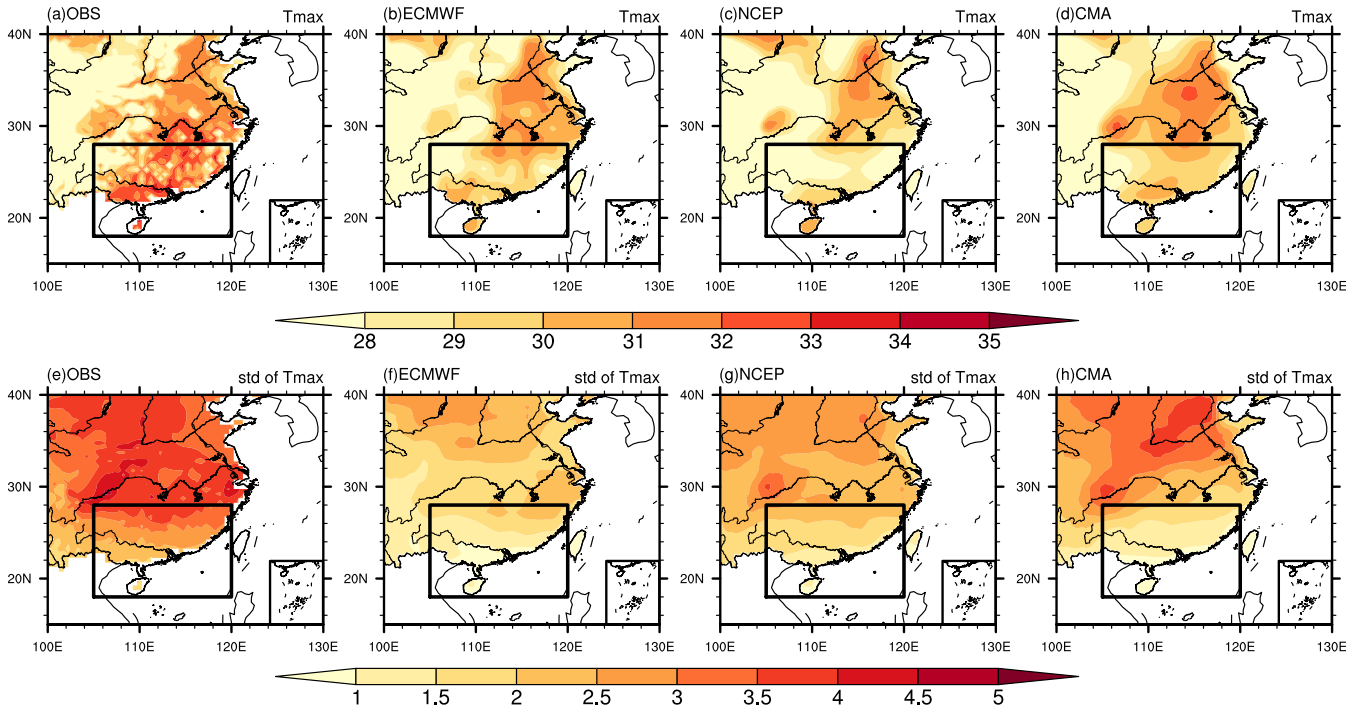

FIGURE 1 Distributions of the climatological (a)–(d) T_{max} and (e)–(h) T_{max} standard deviation in JJA during 1999–2010 (units:°C). The panels from left to right are for the observation and the 10-day-lead ensemble forecasts of the European Centre for Medium-Range Weather Forecasts (ECMWF), National Centers for Environmental Prediction (NCEP), and China Meteorological Administration (CMA) models, respectively. The black rectangles denote the domain of South China.

HSS, for example, the HSSs for all three models drop dramatically with increasing lead time, with basically no forecasting skill after 15-day leads. Before 15-day leads, ECMWF shows the highest forecast skill, NCEP the second, and CMA the lowest. Taking 10-day leads, for example, the HSS is 0.31 for ECMWF, 0.09 for NCEP, and 0.07 for CMA. In the following, the results of 10-day leads are employed to assess the extended-range forecast skills.

Table 1 lists the dates of the 17 EHEs in the observation, as well as the predicted dates in models. The ECMWF model correctly predicts seven events, while the NCEP and CMA models both only predict three. For details of the false alarms, the numbers of advanced prediction days are 4 for ECMWF, 8 for NCEP, and 7 for CMA and the delayed prediction days are 7 for ECMWF, 17 for NCEP, and 8 for CMA, respectively. Therefore, the false alarms tend to be delayed predictions in the 17 EHEs, and NCEP is the most likely to delay or overestimate the duration of the events. Beyond those listed in Table 1, the rest numbers of false alarms are 56 for ECMWF, 63 for NCEP, and 79 for CMA. It is indicated that ECMWF has the highest predicting accuracy of EHEs and EHDs. To understand the models' different performances, three events are selected for further analyses. The first is in June 1999, for which ECMWF correctly forecasts all the EHDs and could be a typical case to document its high forecast skill. The second is the most prolonged event that happened in August 2009, considering the urgent need for an accurate forecast of such extreme cases. The third is during August 3–5, 2010, when NCEP predicts the EHE while ECMWF misses and could illustrate the case failure of ECMWF.

3.2 | The case in June 1999

For the 1999 event, EHDs lasted for 3 days from June 4 to 6 in the observation, with positive T_{max} anomaly increasing since June 1 and dramatically decreasing after June 6 (Figures 3a and S1). The ECMWF model accurately forecasts the EHE, but the T_{max} anomaly starts to decay after June 4, 2 days earlier than the observation. The predicted EHDs of NCEP and CMA are later than the observation, starting from June 5. Then, the T_{max} anomalies keep at a large amplitude for the two models, resulting in delayed EHDs prediction.

The T_{max} biases in the model are intimately related to the circulation biases. Figure 4 demonstrates the evolution of 500-hPa circulation anomalies. In the observation, an anomalous high accompanied by an anticyclonic anomaly occurs over South China on June 1, and then strengthens and propagates northward (Figure 4a1–f1).

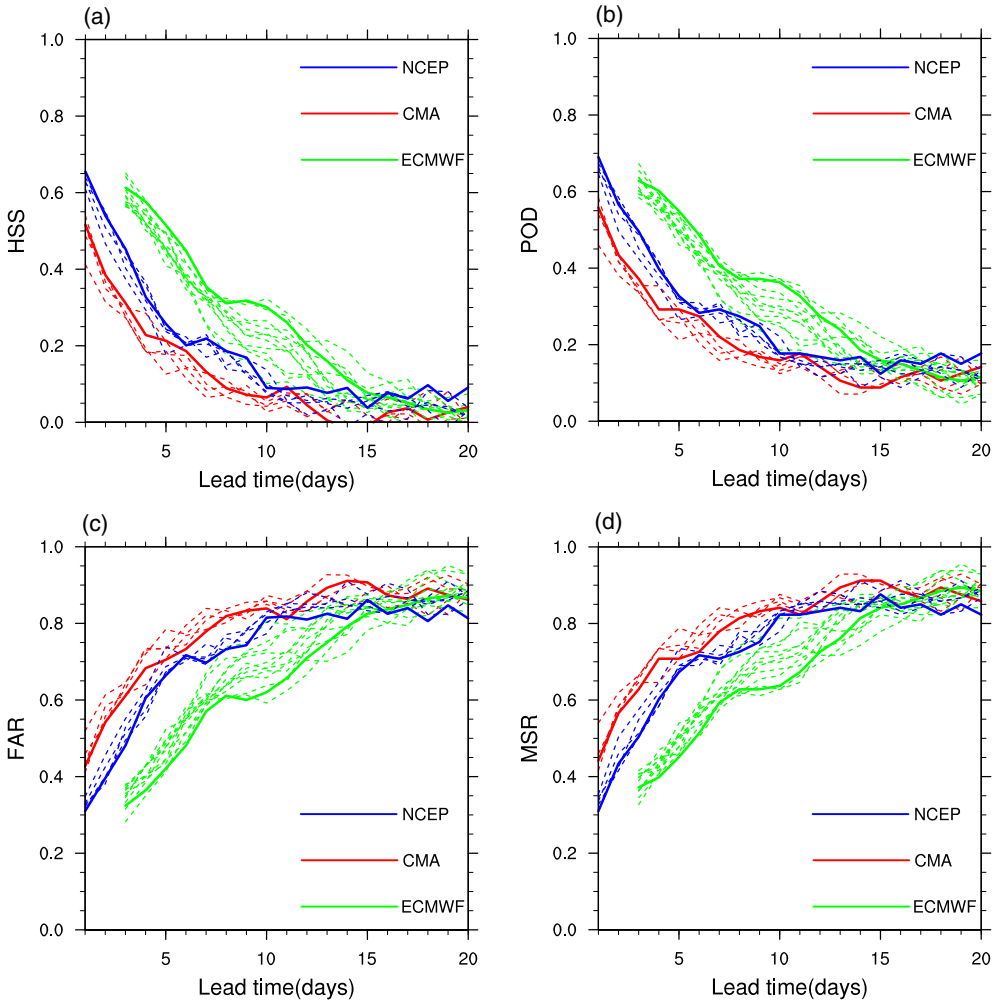

FIGURE 2 The (a) Heidke skill score (HSS), (b) probability of detection (POD), (c) false-alarm rate (FAR), and (d) miss rate (MSR) of extreme heat days predictions at different forecast lead times from 1 to 20 days (*x*-axis) for the individual members (dashed lines) and the ensemble (solid lines) forecast of the European Centre for Medium-Range Weather Forecasts (ECMWF) (green), National Centers for Environmental Prediction (NCEP) (blue), and China Meteorological Administration (CMA) (red) models.

The anticyclonic anomaly favors the warming over South China, by inducing not only anomalous subsidence accompanied by adiabatic heating but also anomalous dry conditions accompanied by reduced cloud cover and enhanced insolation to heat the surface (Chen et al., 2018; Lin, Chen, et al., 2022). During June 5 and 6, another anomalous anticyclone originating from the mid-latitudes propagates southeastward to merge with the previous one and thus strengthens the anticyclonic anomaly (Figure 4e1,f1), enhancing the T_{max} over South China. On the other hand, an anomalous low accompanied by a cyclonic anomaly originating from the Philippines moving northward since June 1, which affected the coast of South China on June 6 (Figure 4a1–-f1). The arrival of cyclonic anomaly causes the decay of high temperature (Figure 4g1,h1).

The ECMWF model could well predict the anticyclonic–cyclonic pair propagating northward from the tropics (Figure 4a2–h2). However, the anomalous high around South China is generally weaker in the model, leading to a smaller T_{max} anomaly. Moreover, the model fails to predict the move-in of the mid-latitude anticyclone during June 5 and 6 (Figure 4e2,f2), thus misses the continuous T_{max} enhancement in these days. NCEP could overall capture the tropical anticyclonic–cyclonic anomalies, but the anomalous high around South China is obviously weaker than the observation (Figure 4a3–h3). Moreover, the northward-propagating speed of the tropical anomaly is slower, which is about 0.8°latitude/day in NCEP while 1.7°and 1.6°latitude/day in the observation and ECMWF (Figure S4a1–c1). During June 6–8, the anomalous tropical cyclone gradually moved into South China and resulted in T_{max} decaying in the observation (Figure 4f1–h1), but still stays over the ocean and South China is dominated by anticyclone and thus high T_{max} anomaly in the NCEP model (Figure 4f3–h3). In addition, albeit the model predicts a mid-latitude anticyclonic anomaly from June 4 to 8, the anticyclone does not move to merge with the tropical one until June 8. For CMA, it fails to capture the northward-propagating anticyclonic–cyclonic pair from the tropics (Figure 4a4–h4). The anomalous high-causing EHDs mainly come from the west, which gradually strengthens and propagates eastward since June 3 and results in the falsely delayed T_{max} rising (Figure 4c4–h4).

TABLE 1 The dates of the 17 EHEs in the observation (Column 1), and the dates predicted by the ECMWF (Column 2), NCEP (Column 3), and CMA (Column 4) models (only the periods from 3 days before to 3 days after the observed events are counted).

OBS	ECMWF	NCEP	CMA
Jun 4–6, 1999	[Jun 4–6]	Jun 5, 7, 8	[Jun 5, 6, 8]
Jun 2–5, 2000	[Jun 1, 2–5, 6–8]	[Jun 2–5, 7]	[Jun 3, 4]
Jun 29–Jul 1, 2000	None	Jul 1	None
Jul 26–29, 2000	None	None	None
Jun 5–8, 2002	None	None	[Jun 3, 6, 7, 11]
Jul 13–15, 2002	None	Jul 10, 11, 14, 16	None
Jul 14–19, 2003	[Jul 12, 13, 14, 16–19, 20, 21]	None	Jul 11–13, 17, 18
Jul 28–Aug 4, 2003	[Jul 28, 29, Aug 1–4]	Jul 25–27, 29–31, Aug 6, 7	Jul 25, 30, Aug 6, 7
Jun 28–Jul 3, 2004	Jun 28, Jul 2	None	Jul 2, 6
Aug 9–11, 2004	[Aug 10, 11]	Aug 11, 12–16	None
Jul 16–18, 2005	None	Jul 19	Jul 14, 15, 16
Jun 21–24, 2007	Jun 19, 22	[Jun 19, 20, 21–24, 25]	Jun 21, 25
Jun 18–21, 2009	None	None	Jun 21
Aug 19–29, 2009	[Aug 19, 22, 23, 26–29, 30, 31]	None	Aug 28, 29, 31
Jul 1–5, 2010	[Jul 1, 2, 4, 5]	None	None
Aug 3–5, 2010	None	[Aug 4, 5, 6]	None
Aug 9–11, 2010	None	Aug 6, 12–14	None

Note: Green dates represent the correct predictions, blue and red dates represent the advanced and delayed predictions of the false alarms, respectively. Brackets indicate the correctly predicted EHEs.

Abbreviations: CMA, China Meteorological Administration; ECMWF, European Centre for Medium-Range Weather Forecasts; EHE, extreme heat event; NCEP, National Centers for Environmental Prediction.

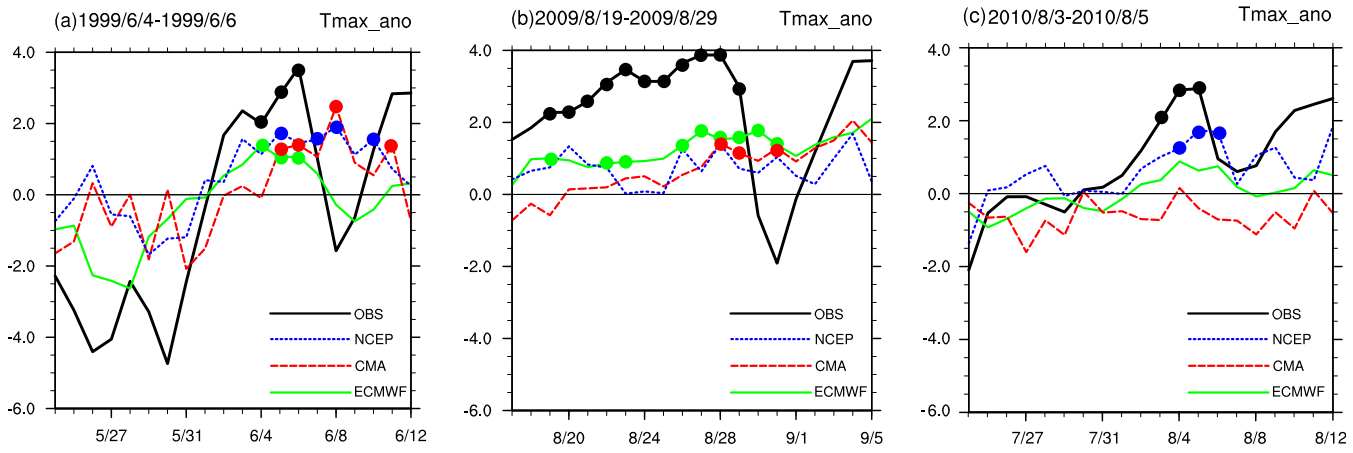

FIGURE 3 Temporal evolution of the T_{max} anomalies over South China for the (a) 1999, (b) 2009, and (c) 2010 extreme heat events (units:°C). Black lines represent the observations. Green, blue, and red lines represent the 10-day-lead predictions by the European Centre for Medium-Range Weather Forecasts (ECMWF), National Centers for Environmental Prediction (NCEP), and China Meteorological Administration (CMA) models, respectively. Dots denote the observed and model-predicted extreme heat days.

Briefly, the 1999 EHE case over South China is mainly influenced by a pair of anticyclonic–cyclonic anomalies from the tropics and an additional mid-latitude anticyclonic anomaly from the north. ECMWF could well forecast the propagation of the tropical circulation and the resultant EHDs. NCEP could capture the tropical circulation, but with slower northward propagation and falsely continued prediction of EHDs. CMA could not capture the tropical circulation and forecast delayed EHDs mainly via a false circulation system originating from the west. Meanwhile, all models produce anomalies weaker than the observation and fail

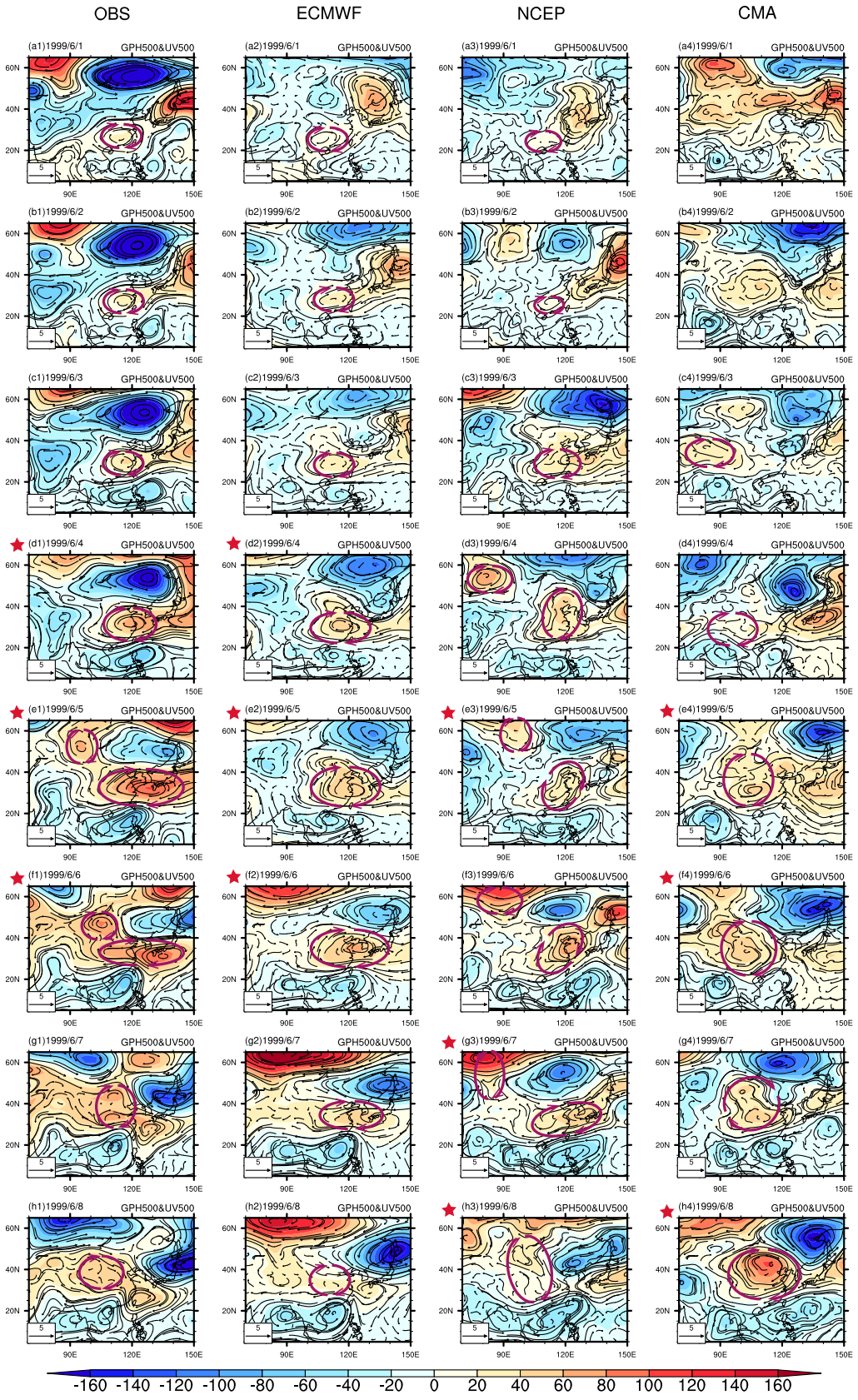

FIGURE 4 Evolution of 500-hPa geopotential height (shadings; units: m) and wind (vectors; units: $m \cdot s^{-1}$) anomalies for the extreme heat event in June 1999. The columns from left to right show the results of (a1–h1) observation, and the 10-day-lead ensemble forecasts of (a2–h2) European Centre for Medium-Range Weather Forecasts (ECMWF), (a3–h3) National Centers for Environmental Prediction (NCEP), (a4–h4) China Meteorological Administration (CMA) models, respectively. Red asterisks mark the identified extreme heat days. The clockwise circles denote the anticyclonic anomalies affecting South China.

to correctly predict the influence of mid-latitude circulation.

3.3 | The case in August 2009

For the 2009 event, EHDs lasted from August 19 to 29 in the observation, with two warming periods during August 19–23 and 25–28 and diminished T_{max} anomaly after August 28 (Figures 3b and S2). ECMWF correctly forecasts most of the EHDs (except August 20, 21, 24, and 25) but falsely lasts for two more days (August 30 and 31). NCEP fails to capture the EHE because the warming amplitude is too small. For CMA, the T_{max} anomaly increases gradually before August 28 and only the last two observed EHDs are correctly predicted. Then, the T_{max} anomaly stays large and leads to a delayed predicted EHD.

In the observation, the EHE onset during the first warming period is caused by an anomalous anticyclone extending from the mid-latitudes to the tropics over East Asia (Figure 5b1), which is merged by two anomalous anticyclones located over the southeastern coast of China and Northeast Asia, respectively (Figure 5a1). Meanwhile, another mid-latitude anomalous anticyclone emerges in the northwest and propagates southeastward to merge with the previous one, forming a prominent mid-latitude anticyclonic anomaly on August 23 (Figure 5b1–d1). During the second warming period, the mid-latitude anomalous anticyclone continues to move southeastward (mainly southward) to affect South China, with its center passing through (Figure 5d1–h1). Albeit originating from different latitudes, previous study indicates that the mid-latitude anticyclonic anomaly favors the EHE in South China via processes similar to the tropical anticyclonic anomaly, including subsiding adiabatic heating and insolation heating (Li & Chen, 2023). The anticyclone basically moves out of South China after August 29 and leads to the cease of EHE (Figure 5h1).

Models could predict a tropical and a mid-latitude anticyclonic anomaly on August 17, but present biases in the subsequent evolution. For ECMWF, during the first warming period, the merged anticyclone is accompanied by obviously weaker high anomaly compared to the observation (Figure 5a2–d2), which would cause the weaker T_{max} anomaly and failed prediction of continuous EHDs over South Chin. During the second warming period, the mid-latitude anticyclonic anomaly moves southward more slowly than observation (Figure 5e2–h2), with a southward-propagating speed of 0.7°latitude/day in ECMWF but 3°latitude/day in the observation (Figure S4a2,b2). As a result, the anticyclonic center is still located around South China from August 27 to 31, preventing T_{max} from decaying quickly as observation. For both NCEP and CMA, during the first warming period, the merged anticyclone is overall located more northward, and the high anomaly over South China is obviously weaker than observation (Figure 5a3–d3,a4–d4), resulting in weaker T_{max} anomaly. During the second warming period, the mid-latitude anticyclone in the NCEP model propagates southward more slowly (0.7°latitude/day; Figure S4c2) but eastward faster compared with observation, thus the anticyclonic center does not move to South China to cause EHD (Figure 5e3–h3). In contrast, CMA is characterized by another anomalous anticyclone propagating eastward from the west, with its center extending to South China since August 29 and causing the delayed EHDs prediction (Figure 5e4–h4).

In short, the 2009 EHE is modulated by an anticyclonic anomaly moving mainly southward from the mid-latitudes. ECMWF has skill in forecasting the mid-latitude circulation but with weaker amplitude and slower southward propagation, resulting in the miss or delay of EHD. The forecast skill of the mid-latitude circulation for NCEP is worse, which presents weaker amplitude and biases in the propagating speed and direction. Albeit CMA could predict some EHDs, its predicting skill of the mid-latitude circulation seems to be the worst, which features weaker amplitude and even a wrong anticyclonic anomaly originating from the west.

3.4 | The case in August 3–5, 2010

In the 2010 event, EHDs lasted for 3 days from August 3 to 5 in the observation, with positive T_{max} anomaly increasing since August 1 and dramatically decreasing after August 5 (Figures 3c and S3). The predicted EHDs of the NCEP model are 1 day later than the observation, persisting from August 4 to 6. The ECMWF model fails to capture the EHE because the warming amplitude is too small, while the CMA model predicts a negative T_{max} anomaly.

In the observation, the EHE onset on August 3 is caused by an anomalous anticyclone merged by anomalies from the mid-latitudes and tropics (Figure 6a1–c1). During August 3–5, the anomalous high center associated with the anticyclone extends to South China and propagates southward (Figure 6c1–e1). After August 5, the anomalous anticyclone propagates eastward and leads to the cease of EHE (Figure 6f1–h1). For ECMWF, it could predict the precursory merging of the mid-latitude and tropical anticyclonic anomaly but with a smaller high-pressure anomaly (Figure 6a2,b2). Moreover, the merged anticyclone moves southward obviously more slowly

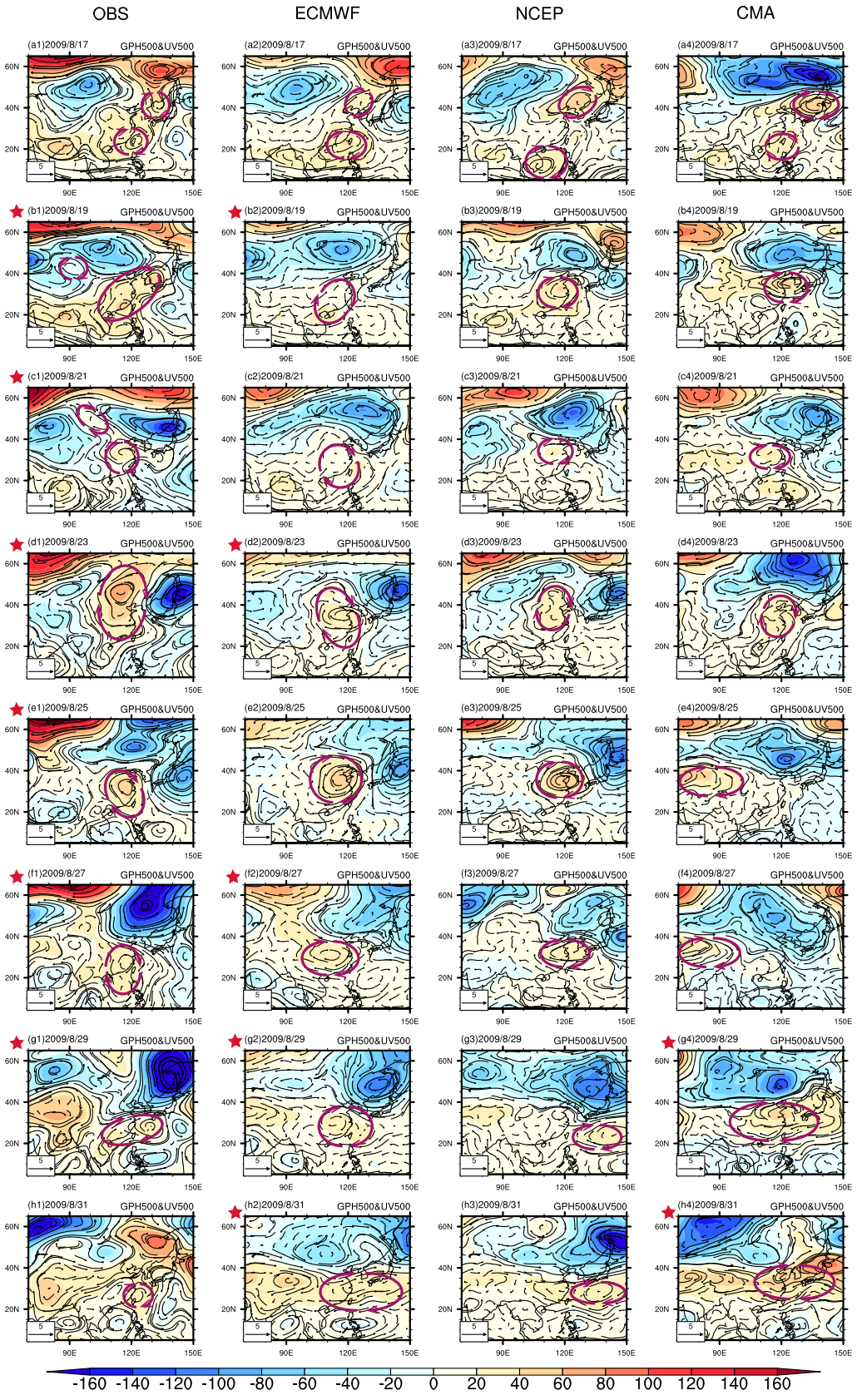

FIGURE 5 Evolution of 500-hPa geopotential height (shadings; units: m) and wind (vectors; units: $m \cdot s^{-1}$) anomalies for the extreme heat event in August 2009. The columns from left to right show the results of (a1–h1) observation, and the 10-day-lead ensemble forecasts of (a2–h2) European Centre for Medium-Range Weather Forecasts (ECMWF), (a3–h3) National Centers for Environmental Prediction (NCEP), (a4–h4) China Meteorological Administration (CMA) models, respectively. Red asterisks mark the identified extreme heat days. The clockwise circles denote the anticyclonic anomalies affecting South China.

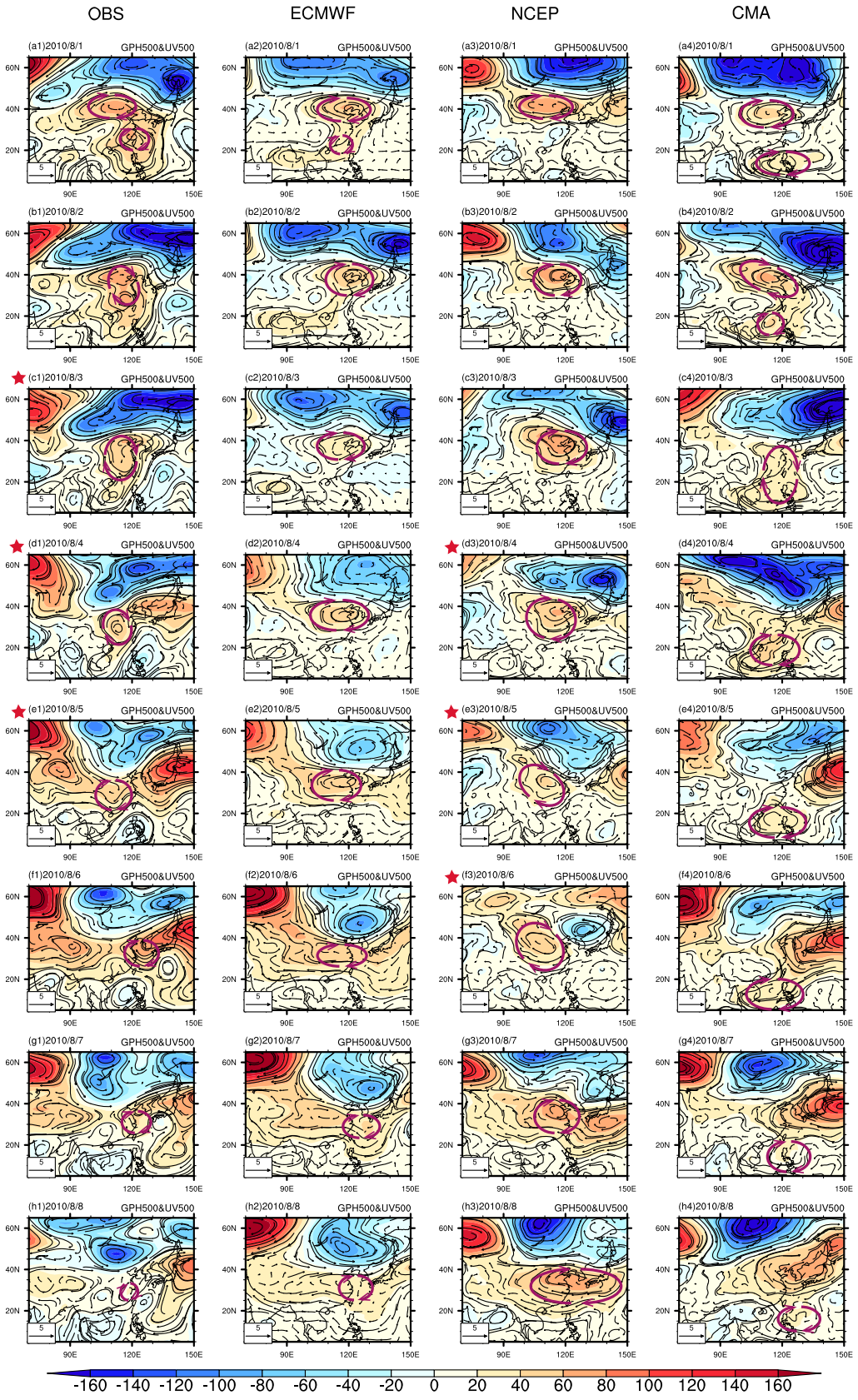

FIGURE 6 Evolution of 500-hPa geopotential height (shadings; units: m) and wind (vectors; units: $m \cdot s^{-1}$) anomalies for the extreme heat event in August 2010. The columns from left to right show the results of (a1–h1) observation, and the 10-day-lead ensemble forecasts of (a2–h2) European Centre for Medium-Range Weather Forecasts (ECMWF), (a3–h3) National Centers for Environmental Prediction (NCEP), (a4–h4) China Meteorological Administration (CMA) models, respectively. Red asterisks mark the identified extreme heat days. The clockwise circles denote the anticyclonic anomalies affecting South China.

(1.3°latitude/day) than the observation (2°latitude/day) (Figures 6c2–h2 and S4a3,b3), with the anomalous high centered north to South China and leading to the miss of EHDs. For NCEP, the mid-latitude anticyclonic anomaly is similar to the observation but the tropical anticyclone is missing (Figures 6a3,b3 and S4c3). Due to the absence of tropical anomaly, the anomalous anticyclone is located more northward overall, and thus, its center extends to South China later than the observation (Figure 6c3–h3), causing the delayed predicted EHDs. For CMA, it could predict a mid-latitude and a tropical anticyclonic anomaly on August 1 and 2, but the tropical anomaly is located much more southward (Figure 6a4–b4). The merged anticyclonic anomaly is weaker than the observation and is falsely centered to the southeast of South China (Figure 6c4–h4), failing to cause EHD.

Similar to the 2009 case, the 2010 EHE results from an anticyclonic anomaly propagating southward from the mid-latitudes, which is formed by the merging of a precursory mid-latitude and tropical anticyclonic anomaly. ECMWF could reproduce the formation of the anticyclonic anomaly but presents obviously weaker anomaly and slower southward propagation, leading to the miss of EHE. NCEP could basically capture the mid-latitude anticyclonic anomaly, but misses the precursory tropical anticyclone and leads to the more northward location and later move-in of the anticyclonic center to South China, causing delayed EHDs. As for CMA, the merged anticyclonic anomaly is weaker and falsely located to the southeast of South China, failing to cause EHD.

4 | CONCLUSIONS AND DISCUSSION

The extended-range forecast skills of the EHEs over South China are assessed by three S2S models, including the ECMWF, NCEP, and CMA models. Statistical metrics show that ECMWF has the best forecast skill at most lead times, NECP follows, CMA the poorest, and the 10-day-lead reforecast results are used for further analyses. The false alarms in the models seem to be due to delayed prediction more than advanced prediction in the EHEs, with NCEP presenting the most evident tendency of delayed prediction, ECMWF the second and CMA only a feeble tendency.

Three cases are selected to illustrate the models' different performance. The first is on June 4–6, 1999, for which ECMWF correctly predicts all EHDs, the second is the most prolonged EHE during August 19–29, 2009, and the third is on August 3–5, 2010, for which NCEP predicts the EHE while the other two models fail. The 1999 case is influenced by a pair of tropical anticyclonic–cyclonic anomalies propagating northward and an additional mid-latitude anticyclonic anomaly propagating southward. The 2009 and 2010 cases are modulated by the southward movement of a mid-latitude anticyclonic anomaly that merged with a precursory mid-latitude and tropical anticyclone. Overall, the predicted circulation anomalies in models are weaker than the observation, resulting in their weaker T_{max} anomalies and misses of some EHDs. For ECMWF, it predicts the tropical circulation and resultant EHDs in the 1999 case, captures the mid-latitude circulation but with slower propagation and thus falsely continued prediction of EHDs in the 2009 case, reproduces the formation of mid-latitude anticyclone but with slower propagation and misses the EHDs in the 2010 case. NCEP captures the tropical circulation but with slower propagation and delayed EHDs in the 1999 case, produces the mid-latitude signal but propagates with slower speed and deviated direction and fails to induce EHD in the 2009 case, captures the mid-latitude anticyclonic anomaly but misses the precursory tropical signal and leads to the more northward anticyclone and delayed EHDs in the 2010 case. For CMA, it predicts some EHDs in the former two cases but via a false anticyclonic anomaly originating from the west, misses the EHE in the last case due to the false location of the anticyclone.

Overall, in the selected cases, ECMWF has better skill in predicting the tropical circulation than the mid-latitude circulation, NCEP has biases in the propagation of both the tropical and mid-latitude circulation, while CMA tends to falsely predict the origin or location of the circulation anomaly. These results reveal some potential disadvantages that the models need to overcome to improve their extended-range forecast skills. However, more cases and more models are required to comprehensively assess our current forecast skills of EHEs.

The models' different forecast skills might be partly due to their operation manners and settings (Table S1). Different from the fixed reforecasts of NCEP and CMA models, which are produced once, the on-the-fly reforecast of ECMWF is produced every week starting the same day and same month as the next real-time forecast and using an updated model version. The updates in initialization and model might contribute to the better skill of ECMWF. Moreover, ECMWF has larger ensemble members and finer resolution, which might further benefit its better skill. The finer vertical resolution of NCEP than CMA might contribute to the better skill for the former. Other differences among the models such as the physical processes might also be critical in determining their forecast skills.

AUTHOR CONTRIBUTIONS

Xiaoqi Li: Writing – original draft; formal analysis. **Ruidan Chen:** Writing – original draft; writing – review and editing; supervision. **Yunting Qiao:** Writing – review and editing.

ACKNOWLEDGEMENTS

This study is supported by the Joint Funds of the National Natural Science Foundation of China (U2342205), National Natural Science Foundation of China (42375028), Innovation Group Project of Southern Marine Science and Engineering Guangdong Laboratory (Zhuhai) (No. 316323005), and the Science and Technology Planning Project of Guangdong Province (2023B1212060019).

CONFLICT OF INTEREST STATEMENT

The authors declare no conflict of interest.

DATA AVAILABILITY STATEMENT

All data used in the study are freely available, with the links listed below: CN05 temperature: https://data.cma.cn. NCEP reanalysis: https://psl.noaa.gov/data/gridded/data.ncep.reanalysis.derived.html. S2S reforecast: http://apps.ecmwf.int/datasets/data/s2s.

ORCID

Ruidan Chen https://orcid.org/0000-0001-6207-8805

REFERENCES

Chen, R. & Lu, R. (2015) Comparisons of the circulation anomalies associated with extreme heat in different regions of eastern China. *Journal of Climate*, 28, 5830–5844. Available from: https://doi.org/10.1175/JCLI-D-14-00818.1

Chen, R., Wen, Z. & Lu, R. (2018) Interdecadal change on the relationship between the mid-summer temperature in South China and atmospheric circulation and sea surface temperature. *Climate Dynamics*, 54, 2113–2126. Available from: https://doi.org/10.1007/s00382-017-4002-5

Gao, M., Wang, B., Yang, J. & Dong, W. (2018) Are peak summer sultry heat wavedays over Yangtze–Huaihe River basin predictable? *Journal of Climate*, 31, 2185–2196. Available from: https://doi.org/10.1175/JCLI-D-17-0342.1

Heidke, P. (1926) Berechnung Des Erfolges und der güte der windstärkevorhersagen im sturmwarnungsdienst. *Geografiska Annaler*, 8, 301–349. Available from: https://doi.org/10.1080/20014422.1926.11881138

Hsu, P., Li, T., You, L., Gao, J. & Ren, H.-L. (2015) A spatial–temporal projection model for 10–30 day rainfall forecast in South China. *Climate Dynamics*, 44, 1227–1244. Available from: https://doi.org/10.1007/s00382-014-2215-4

IPCC. (2023) Weather and climate extreme events in a changing climate. In: *Climate change 2021: The physical science basis*. Cambridge: Cambridge University Press, pp. 1513–1766. Available from: https://doi.org/10.1017/9781009157896.013

Kalnay, E., Kanamitsu, M., Kistler, R., Collins, W., Deaven, D., Gandin, L. et al. (1996) The NCEP/NCAR 40-year reanalysis project. *Bulletin of the American Meteorological Society*, 77, 437–471.

Li, X. & Chen, R. (2023) Diversity in the quasi-biweekly oscillation sources of the daily maximum temperature over South China during summer. *International Journal of Climatology*, 43, 7099–7118. Available from: https://doi.org/10.1002/joc.8254

Li, Y., Xu, K., Wu, Z., Zhu, Z. & Wang, Q.J. (2023) A statistical–dynamical approach for probabilistic prediction of sub-seasonal precipitation anomalies over 17 hydroclimatic regions in China. *Hydrology and Earth System Sciences*, 27, 4187–4203. Available from: https://doi.org/10.5194/hess-27-4187-2023

Lin, H., Mo, R. & Vitart, F. (2022) The 2021 western North American heatwave and its subseasonal predictions. *Geophysical Research Letters*, 49, e2021GL097036. Available from: https://doi.org/10.1029/2021GL097036

Lin, W., Chen, R., Wen, Z. & Chen, W. (2022) Large-scale circulation features responsible for different types of extreme high temperatures with extreme coverage over South China. *International Journal of Climatology*, 42(2), 974–992. Available from: https://doi.org/10.1002/joc.7283

Qi, X. & Yang, J. (2019) Extended-range prediction of a heat wave event over the Yangtze River Valley: role of intraseasonal signals. *Atmospheric and Oceanic Science Letters*, 12, 451–457. Available from: https://doi.org/10.1080/16742834.2019.1669408

Vitart, F., Ardilouze, C., Bonet, A., Brookshaw, A., Chen, M., Codorean, C. et al. (2017) The subseasonal to seasonal (S2S) prediction project database. *Bulletin of the American Meteorological Society*, 98(1), 163–173. Available from: https://doi.org/10.1175/BAMS-D-16-0017.1

Vitart, F. & Robertson, A.W. (2018) The sub-seasonal to seasonal prediction project (S2S) and the prediction of extreme events. *npj Climate and Atmospheric Science*, 1, 3. Available from: https://doi.org/10.1038/s41612-018-0013-0

Wang, C., Zheng J., Lin W. & Wang Y. (2023) Unprecedented heatwave in western North America during late June of 2021: Roles of atmospheric circulation and global warming. *Advances in Atmospheric Sciences*, 40, 14–28. Available from: https://doi.org/10.1007/s00376-022-2078-2

Weaver, S.J., Kumar, A. & Chen, M. (2014) Recent increases in extreme temperature occurrence over land. *Geophysical Research Letters*, 41, 4669–4675. Available from: https://doi.org/10.1002/2014GL060300

White, C.J., Domeisen, D.I., Acharya, N., Adefisan, E.A., Anderson, M.L., Aura, S. et al. (2022) Advances in the application and utility of subseasonal-to-seasonal predictions. *Bulletin of the American Meteorological Society*, 103, E1448–E1472. Available from: https://doi.org/10.1175/BAMS-D-20-0224.1

Wulff, C.O. & Domeisen, D.I.V. (2019) Higher subseasonal predictability of extreme hot European summer temperatures as compared to average summers. *Geophysical Research Letters*, 46(20), 11520–11529. Available from: https://doi.org/10.1029/2019gl084314

Xie, J., Yu, J., Chen, H. & Hsu, P.-C. (2020) Sources of subseasonal prediction skill for heatwaves over the Yangtze River basin revealed from three S2S models. *Advances in Atmospheric Sciences*, 37(12), 1435–1450. Available from: https://doi.org/10.1007/s00376-020-0144-1

Xu, Y., Gao, X., Shen, Y., Xu, C., Shi, Y. & Giorgi, F. (2009) A daily temperature dataset over China and its application in validating a

RCM simulation. *Advances in Atmospheric Sciences*, 26(4), 763–772. Available from: https://doi.org/10.1007/s00376-009-9029-z

Yang, J., Zhu, T., Gao, M., Lin, H., Wang, B. & Bao, Q. (2018) Late-July barrier for subseasonal forecast of summer daily maximum temperature over Yangtze River Basin. *Geophysical Research Letters*, 45, 12610–12615. Available from: https://doi.org/10.1029/2018GL080963

Zhang, D.Q., Zheng, Z.H., Chen, L.J. & Zhang, P.Q. (2019) Advances on the predictability and prediction methods of 10-30 d extended range forecast. *Journal of Applied Meteorological Science*, 30(4), 416–430.

Zhang, Q., Sun, G., Dai, G. & Mu, M. (2024) Impact of uncertainties in land surface processes on subseasonal predictability of heat waves onset over the Yangtze River Valley. *Journal of Geophysical Research: Atmospheres*, 129, e2023JD038674. Available from: https://doi.org/10.1029/2023JD038674

Zheng, J. & Wang, C. (2019) Hot summers in the Northern Hemisphere. *Geophysical Research Letters*, 46, 10891–10900. Available from: https://doi.org/10.1029/2019GL084219

Zhu, Z. & Li, T. (2018) Extended-range forecasting of Chinese summer surface air temperature and heat waves. *Climate Dynamics*, 50(5-6), 2007–2021. Available from: https://doi.org/10.1007/s00382-017-3733-7

SUPPORTING INFORMATION

Additional supporting information can be found online in the Supporting Information section at the end of this article.

How to cite this article: Li, X., Chen, R., & Qiao, Y. (2024). Assessing the extended-range forecast skills of the extreme heat events over South China based on three S2S models. *Atmospheric Science Letters*, *25*(9), e1253. https://doi.org/10.1002/asl.1253